

Efficient Pairwise Neuroimage Analysis using the Soft Jaccard Index and 3D Keypoint Sets

Laurent Chauvin, Kuldeep Kumar, Christian Desrosiers, William Wells III and Matthew Toews

Abstract—We propose a novel pairwise distance measure between variable-sized sets of image keypoints for the purpose of large-scale medical image indexing. Our measure generalizes the Jaccard index to account for soft set equivalence (SSE) between set elements, via an adaptive kernel framework accounting for uncertainty in keypoint appearance and geometry. Novel kernels are proposed to quantify the variability of keypoint geometry in location and scale. Our distance measure may be estimated between N^2 image pairs in $O(N \log N)$ operations via keypoint indexing. Experiments validate our method in predicting 509,545 pairwise relationships from T1-weighted MRI brain volumes of monozygotic and dizygotic twins, siblings and half-siblings sharing 100%-25% of their polymorphic genes. Soft set equivalence and keypoint geometry kernels outperform standard hard set equivalence (HSE) in predicting family relationships. High accuracy is achieved, with monozygotic twin identification near 100% and several cases of unknown family labels, due to errors in the genotyping process, are correctly paired with family members. Software is provided for efficient fine-grained curation of large, generic image datasets.

Index Terms—neuroimage analysis, invariant keypoints, MRI

I. INTRODUCTION

HEALTH treatment is increasingly personalized, where treatment decisions are conditioned on patient-specific information in addition to knowledge regarding the general population [1]. Modern genetic testing allows us, based on large libraries of human DNA samples, to cheaply predict patient-specific characteristics, including immediate family relationships, and also characteristics shared across the population including racial ancestry, sex, hereditary disease status, etc. [2], [3]. The brain, the center of cognition, is a complex organ tightly coupled to the genetic evolution of animals and in particular that of the human species. To what degree is the human brain phenotype coupled to the underlying genotype? How does the brain image manifold vary locally with genotype, i.e. immediate relatives sharing 25-100% of their polymorphic genes, or between broad groups defined by subtle genetic factors such as racial ancestry origin or sex?

Large, publicly available databases allow us investigate these questions from aggregated MRI and genetic data of 1000+ subjects [4]. Brain shape has been modeled as lying on a smooth manifold in high dimensional MRI data space [5], [6], where phenotype can be described as a smooth deformation conditioned on developmental factors determined by the environment. However the brain is naturally described as a rich

collection of spatially localized neuroanatomical structures, including common structures such as the basal ganglia shared across the population, but also highly specific patterns such as cortical folds [7] that may only be observable in specific individuals or close family members.

The image keypoint representation is an intuitively appealing means of modeling specific, localized phenomena, where the image is described as a set of descriptors identified at salient image keypoints as shown in Figure 1. A keypoint set can be viewed as an element of a high-dimensional manifold, and medical imaging applications such as regression or classification can be formulated in terms of a suitable geodesic distance between sets. As keypoint sets are variable sized, typical metrics based on fixed-length vectors such as L-norms [5], [6] do not readily apply. Distances defined based on the Jaccard index or intersection-over-union [8] have proven to be effective in recent studies investigating genetics and brain MRI [9], [10]. For example, by defining set equivalence in terms of nearest neighbor (NN) descriptor correspondences, the Jaccard distance may be used to predict pairwise relationships. Nevertheless, the assumption of binary or hard set equivalence (HSE) between keypoints is a crude approximation given probabilistic uncertainty inherent to natural image structure, and is ill-defined for variable sized datasets where the number of nearest neighbor correspondences may be variable or unknown a-priori.

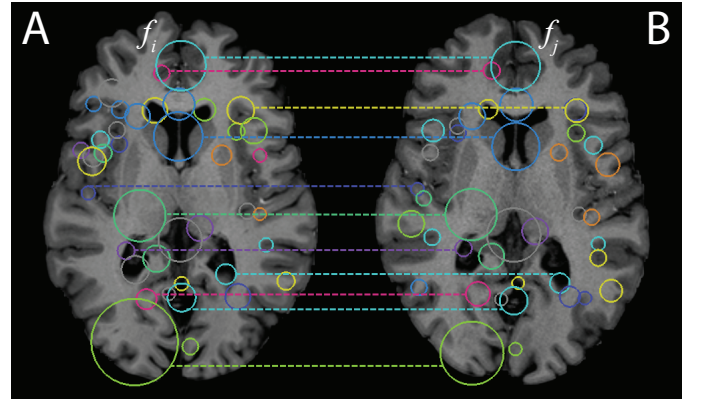


Fig. 1. Illustrating two sets of 3D keypoints $A = \{f_i\}$ and $B = \{f_j\}$ extracted from MRI brain volumes of monozygotic twins. Colored circles represent the 3D locations $\bar{x} \in R^3$, scales (radii) $\sigma \in R^1$ of keypoints in 2D axial slices, and links are correspondences identified via the SIFT-Rank [11] algorithm, note the high degree of local similarity. Colors are assigned for visualization purposes.

Our primary contribution is to introduce a new Jaccard-like measure between pairs of 3D keypoint sets, based on

L. Chauvin, K. Kumar, C. Desrosiers and M. Toews are with the Ecole de Technologie Supérieure, Montreal, Canada

W. Wells is with the Harvard Medical School and the Massachusetts Institute of Technology, Boston, USA

probabilistic or soft set equivalence (SSE), overcoming the limitations of hard equivalence. SSE is achieved via an adaptive kernel [12] accounting for uncertainty in both local keypoint appearance and geometry, and automatically adapting to the quantity of available data. A novel kernel is introduced that normalizes variability in pairwise keypoint displacement by the geometrical mean of keypoint scales, accounting for localization uncertainty in scale-space. This work extends keypoint-based neuroimaging analysis methods based on hard set equivalence (HSE) and appearance descriptors [9], [10], [13].

Experimentally, our work builds upon the keypoint signatures approach [10], the first to report perfect accuracy at identifying repeat scans of the same individuals and instances of previously unknown subject labeling consistencies in widely used, public neuroimage MRI datasets (e.g. OASIS [14], ADNI [15], HCP [16]). Here, following from preliminary work [17], we present a kernel-based formulation of the soft Jaccard index along with a novel geometrical kernel in 3D metric space, and demonstrate their importance in fine-grained analysis of human sibling relationships.

II. RELATED WORK

Our work is motivated both by the study of the link between genotype and brain phenotype in the human brain from large datasets [18], and by practical applications such as maintaining accurate patient records in hospital Picture Archiving and Communication Systems (PACS). We adopted a memory-based learning model where all data are stored in memory and accessed via highly-specific keypoint queries. Memory-based learning requires no explicit training procedure [19], and the accuracy approaches Bayes optimality as the number of data N becomes large [20]. 3D SIFT keypoints [11] derived from Gaussian scale-space theory [21], [22] are invariant to global similarity transforms and contrast variations, and thus account for misalignment and scanner variability between images. Efficient indexing reduces the quadratic $O(N^2)$ complexity of nearest neighbor (NN) keypoint lookup to $O(N \log N)$, e.g. via $O(\log N)$ KD-tree indexing [23], ensuring that the method scales gracefully to large datasets, e.g. 7500 brain MRIs [24] or 20000 lung CTs [25].

Keypoint sets for different images generally do not contain the same numbers of elements, and a natural choice for pairwise distance between variable sized sets are measures based on set intersection or overlap, e.g. the Jaccard distance metric [8] first proposed in [26] or the Tanimoto distance [27], [28]. In medical image analysis, the Jaccard distance has been used to assess pixel-level segmentation accuracy [29], and has proven highly effective for pairwise neuroimage similarity based on 3D SIFT keypoint data [9], [13], where set equivalence is determined by nearest neighbor keypoint descriptors. Soft set theory has been investigated in various works, e.g. [30]–[32], generally including soft set membership and equivalence in operations on pairs of sets including intersection and union. A Jaccard-like distance was used for retrieving near-duplicate photos [33], where the ratio of soft intersection and union operators was used to account for

inverse document frequency (idf). Our work here extends the Jaccard distance proposed in [10] to include keypoint geometry in 3D Euclidean metric space coordinates, and compares to the HSE Jaccard measure used in [9], [13], showing a significant improvement in predicting family relationships.

The keypoint methodology has a number of advantages, such as robustness to occlusion or missing correspondences, invariance to translation, scaling, rotation and intensity contrast variations between images. While its representation serves as a highly robust and general baseline, the search for an alternative local keypoint detectors and descriptors is the focus of active research, primarily for 2D image detection. We refer the reader to an extensive literature review the topic of traditional hand-crafted solutions [34]. Deep learning of keypoint detectors and descriptors is also a current research focus (e.g. LIFT [35], DISK [36], LF-Net [7], SuperPoint [37]). Nevertheless, a number of factors still make deep keypoint architectures difficult to apply to 3D medical image analysis, e.g. a lack of differentiability, the difficulty of training individual components (i.e. keypoint detector, orientation estimation, descriptor), achieving invariance to rotation or scale changes, the need to train for different imaging modalities and body parts, and biased or insufficient training data. Many learning-based approaches rely on existing keypoint detectors to generate training patch data [35], [37]. While deep learning has revolutionized image classification [38], in the case of keypoint matching, SIFT histogram descriptors and variants (e.g. SIFT-Rank [39], DSP-SIFT [40], RootSIFT [41], PCA-SIFT [42]) remain as effective as descriptors derived from training [43], [44], while requiring no training and few hyperparameter.

Our work adopts the 3D SIFT-Rank [11] representation, a robust, general tool used for a variety of imaging tasks, including registration [11], [45], segmentation [46], classification [25], without the need for context-specific training procedures or data. As in the original 2D SIFT approach, keypoint geometry is represented as a location \bar{x} and scale σ , these are detected as extrema of a difference-of-Gaussian scale-space [21], as $\arg\max_{\bar{x}, \sigma} |I(\bar{x}, \sigma) - I(\bar{x}, \kappa\sigma)|$, approximating the Laplacian-of-Gaussian [22], where $I(\bar{x}, \sigma) = I(\bar{x}) * \mathcal{N}(\bar{x}, \sigma^2)$ represents the image convolved with the Gaussian kernel $\mathcal{N}(\bar{x}, \sigma^2)$. The geometry of a keypoint may thus be characterised as an isotropic Gaussian density centered on \bar{x} with variance σ^2 representing spatial extent σ in 3D Euclidean space. Rotationally symmetric Gaussian filtering and uniformly sampled derivative operators lead to scale and rotation invariance, while avoiding bias due to training procedures [47]. The 3D SIFT-Rank descriptor is a 64-element histogram of rank-ordered oriented gradients (HOG) [11], sampled about a scale-normalized reference frame centered on \bar{x} and quantized uniformly into $2 \times 2 \times 2 = 8$ spatial bins \times 8 orientations. Rank transformation provides invariance to arbitrary monotonic variations of descriptor element values [39].

Experimentally, our work is most closely related to neuro fingerprinting methods [9], [13], [48]–[53], which can be used in investigate fine-grained variability of individuals from large neuroimage MRI datasets [4], [54]. Of these, only the neuroimage signatures method [10] reports perfect accuracy for

individual identification from large datasets. Although voxel-based morphometric analysis may be used to highlight image regions where measurements are correlated with sibling relationships [55], [56], these methods are not specific enough to identify pairwise relationships. A number of methods convert all subject data into fixed-length codes, e.g. Shape-DNA [48] descriptors from segmented neuroanatomical structures known to be present in all subjects, or generally by aggregating keypoint descriptors into global Fisher vectors (FV) [57] or clusters following the bag-of-features model [58]–[60]. In contrast, our approach maintains all original keypoint data, which represent distinctive, general neuroanatomical patterns present in pairs of images of an individual or shared by immediate family members, without the need for extensive image pre-processing, segmentation or parcellation maps.

A number of references have investigated predicting family relationships from other modalities other than 3D MRI, particularly 2D face photographs, based on clustering [61], deep neural networks [62], discriminant analysis [63] across expressions and lighting conditions [64]. Accuracy is not generally available for siblings based on genotyping, and no current literature reports near 100% accuracy for monozygotic twin identification from face photographs.

III. METHOD

We seek a pairwise distance measure between two sets $A = \{f_i\}$ and $B = \{f_j\}$ that can be used to estimate proximity and thus genetic relationships between subjects from image data. We begin by describing our method in terms of general set theory, then later include details pertaining to set elements f_i defined as 3D image keypoints. Our measure begins with the Jaccard index or intersection-over-union $J_{HSE}(A, B)$ defined as

$$J_{HSE}(A, B) = \frac{|A \cap B|}{|A| + |B| - |A \cap B|}, \quad (1)$$

where in Equation (1), $J_{HSE}(A, B)$ is defined by binary or hard equivalence between set elements. $A \cap B$ is the intersection operator between sets A and B , and $|A \cap B|$, $|A| = |A \cap A|$, $|B| = |B \cap B|$ represent set cardinality operators that count the numbers of elements present in each set, where $|A \cap B| \leq \min\{|A|, |B|\}$. The Jaccard index is a similarity measure, and may be used to define various distance measures including Jaccard distance metric [8] $1 - J_{HSE}(A, B)$ or the Tanimoto distance measure $-\log J_{HSE}(A, B)$.

In the case of sets of real data samples, for example keypoint descriptors, binary equivalence may be difficult to establish due noise or uncertainty in the measurement process, and we seek to redefine $J_{HSE}(A, B)$ in Equation (1) such that it more accurately accounts for non-binary equivalence between set elements. This may generally be accomplished by redefining the hard set intersection cardinality operator $|A \cap B|$ in Equation (1) by a soft $\mu(A \cap B)$, leading to the following expression for our proposed Jaccard index based soft set equivalence $J_{SSE}(A, B)$

$$J_{SSE}(A, B) = \frac{\mu(A \cap B)}{\mu(A) + \mu(B) - \mu(A \cap B)}. \quad (2)$$

In Equation (2), $J_{SSE}(A, B)$ is defined by the soft cardinality operator $\mu(A \cap B)$, including operator $\mu(A) = \mu(A \cap A)$, $\mu(B) = \mu(B \cap B)$, in a form analogous to hard equivalents. In order to ensure that J_{SSE} remains bounded to the range $[0, 1]$, it is important that $\mu(A \cap B)$ be upper bounded by the minimum of the individual soft set cardinalities $\mu(A \cap B) \leq \min\{\mu(A), \mu(B)\}$. The J_{SSE} is defined by the cardinality of the soft intersection $\mu(A \cap B)$ described in the following section.

Defining $\mu(A \cap B)$: The cardinality of soft set intersection $\mu(A \cap B)$ is intended to reflect the uncertainty in equivalence between set elements $f_i \in A$ and $f_j \in B$. We define equivalence between elements $f_i \in A$ and $f_j \in B$ with a similarity function $\mathcal{K}(f_i, f_j)$ ranging from $[0, 1]$, where $\mathcal{K}(f_i, f_j) = 1$ indicates exact equivalence and $\mathcal{K}(f_i, f_j) = 0$ represents the absence of equivalence. We then define a measure $\mu(A \rightarrow B)$ over a mapping $A \rightarrow B$ from A to B as:

$$\mu(A \rightarrow B) = \sum_i^{|A|} \max_{f_j \in B} \mathcal{K}(f_i, f_j). \quad (3)$$

The similarity function $\mathcal{K}(f_i, f_j)$ in Equation (3) may be generally be defined according to the specific representation of f_i and f_j . The maximum operator $\max_{f_j \in B} \mathcal{K}(f_i, f_j)$ ensures the bound $\mu(A \rightarrow B) \leq \mu(A)$ via a partial injective mapping from A to B , and embodies the intuition that each element $f_i \in A$ has at most one counterpart $f_j \in B$. Equation (3) may be used to define the cardinality of a single set A as $\mu(A) = \mu(A \cap A) = |A|$, which is equivalent for hard and soft cases since for a given $f_i \in A$, $\max_{f_j \in A} \mathcal{K}(f_i, f_j) = \mathcal{K}(f_i, f_i) = 1$ in the case of element f_i . It may also be used to define the cardinality of symmetric soft set intersection as proposed in [30], [32]

$$\begin{aligned} \mu(A \cap B) &= \min \{ \mu(A \rightarrow B), \mu(B \rightarrow A) \}, \\ &= \min \left\{ \sum_i^{|A|} \max_{f_j \in B} \mathcal{K}(f_i, f_j), \sum_j^{|B|} \max_{f_i \in A} \mathcal{K}(f_j, f_i) \right\} \end{aligned} \quad (4)$$

The symmetry of $\mu(A \cap B)$ in Equation (4) ensures that the distance measures derived from the soft Jaccard index such as the Jaccard or Tanimoto distances are semi-metrics. The standard Jaccard index in Equation (1) is thus a special case of the soft Jaccard index in the case of a hard similarity function with a binary-valued kernel $\mathcal{K}(f_i, f_j) \in \{0, 1\}$. In practice, soft set equivalence relaxes the triangle inequality property leading to semi-metric distance measures, and allows us to evaluate the maximum expressions in Equation (4) via nearest neighbor indexing, greatly reducing computational complexity.

Defining $\mathcal{K}(f_i, f_j)$: The soft set intersection cardinality $\mu(A \cap B)$ may be adapted to a specific task by defining $\mathcal{K}(f_i, f_j)$ according to the representation of elements f_i . In the context of this article, a set element f_i is a 3D scale-invariant keypoint $f_i = \{\bar{a}_i, \bar{g}_i\}$ as described in [11], where \bar{g}_i and \bar{a}_i are descriptors of local keypoint geometry and appearance,

respectively. Keypoint geometry $\bar{g}_i = \{\bar{x}_i, \sigma_i\}$ consists of 3D location \bar{x}_i and scale σ_i , and appearance \bar{a}_i is a vector of local image information, here a rank-ordered histogram of oriented image gradients (HOG) [39].

The kernel $\mathcal{K}(f_i, f_j)$ is defined by keypoint elements $f_i = \{\bar{a}_i, \bar{g}_i\} \in A$ and $f_j = \{\bar{a}_j, \bar{g}_j\} \in B$. In the limiting case of a kernel with binary support $\mathcal{K}(f_i, f_j) \in \{0, 1\}$ such as the Iverson bracket $\mathcal{K}(f_i, f_j) = [f_i = f_j]$, the expression in Equation (2) is equivalent to the standard Jaccard with hard set equivalence. Here we relax the assumption of hard equivalence using squared exponential kernels with non-zero support, factored into independent kernels operating separately on local keypoint appearance $\mathcal{K}(\bar{a}_i, \bar{a}_j)$ and geometry $\mathcal{K}(\bar{g}_i, \bar{g}_j)$ variables:

$$\mathcal{K}(f_i, f_j) = \mathcal{K}(\bar{a}_i, \bar{a}_j) \mathcal{K}(\bar{g}_i, \bar{g}_j) \quad (5)$$

The factorization in Equation (5) is due to the use of local appearance descriptors \bar{a}_i that are invariant to 7-parameter similarity transforms of the 3D image coordinate system from which geometry \bar{g}_i is derived. The two kernels in Equation (5) are defined as squared exponential functions as follows.

The appearance kernel $\mathcal{K}(\bar{a}_i, \bar{a}_j)$ is defined by the squared Euclidean distance $\|\bar{a}_i - \bar{a}_j\|_2^2$ between appearance vectors \bar{a}_i and \bar{a}_j :

$$\mathcal{K}(\bar{a}_i, \bar{a}_j) = \exp\left(-\frac{\|\bar{a}_i - \bar{a}_j\|_2^2}{\alpha^2}\right) \quad (6)$$

where in Equation (6), α is an adaptive bandwidth parameter defined as

$$\alpha = \min_{f_j \in \Omega} \|\bar{a}_i - \bar{a}_j\|_2^2, \text{ s.t. } \|\bar{a}_i - \bar{a}_j\|_2^2 > 0, \quad (7)$$

the minimum Euclidean distance between appearance descriptor $\bar{a}_i \in A$ and the nearest descriptor $\bar{a}_j \in \Omega \setminus A$ within the entire available dataset Ω excluding A . This allows the kernel to adapt to arbitrary dataset sizes, shrinking the resolution of prediction as the number of data grows large.

The geometry kernel $\mathcal{K}(\bar{g}_i, \bar{g}_j)$ is novel to this work, and is defined as the product of two kernels, one modulating joint keypoint location and scale $\mathcal{K}(\bar{x}_i, \bar{x}_j, \sigma_i, \sigma_j)$ and the other scale alone $\mathcal{K}(\sigma_i, \sigma_j)$

$$\mathcal{K}(\bar{g}_i, \bar{g}_j) = \mathcal{K}(\bar{x}_i, \bar{x}_j, \sigma_i, \sigma_j) \mathcal{K}(\sigma_i, \sigma_j) \quad (8)$$

These kernels are defined as follows

$$\mathcal{K}(\bar{x}_i, \bar{x}_j, \sigma_i, \sigma_j) = \exp\left(-\frac{\|\bar{x}_i - \bar{x}_j\|_2^2}{\sigma_i \sigma_j}\right) \quad (9)$$

$$\mathcal{K}(\sigma_i, \sigma_j) = \exp\left(-\log^2\left(\frac{\sigma_i}{\sigma_j}\right)\right) \quad (10)$$

Kernel $\mathcal{K}(\bar{x}_i, \bar{x}_j, \sigma_i, \sigma_j)$ in Equation (9) penalizes the squared distance between keypoint coordinates within a local reference frame, normalized by a variance proportional to the product of squared keypoint scales $\sigma_i^2 \sigma_j^2$. This variance embodies uncertainty in keypoint location due to scale, and has a computational form that is reminiscent of mass in Newton's law of gravitation or electric charge magnitude in Coulomb's law. Figure 2 demonstrates the role of this kernel variance in

normalizing higher localization error associated with keypoints of larger scale. Kernel $\mathcal{K}(\sigma_i, \sigma_j)$ in Equation (10) penalizes multiplicative difference between keypoint scales (σ_i, σ_j) .

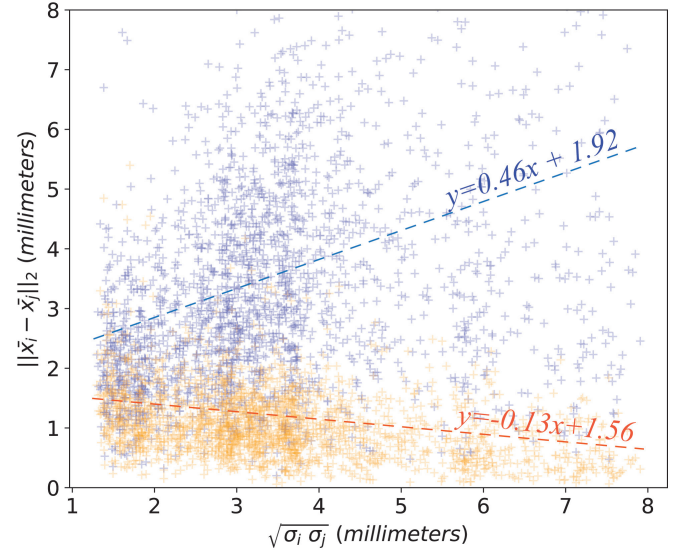


Fig. 2. The graph of spatial localization error $\|\bar{x}_i - \bar{x}_j\|_2$ vs. geometric mean $\sqrt{\sigma_i \sigma_j}$ of scales. Lines represent the linear regression based on each point set. Note how location error increases with scale (blue) due to uncertainty, however this effect (orange) is reduced by normalization in equation (9). This visualization is based feature correspondences between a 10 MRI volumes registered to the same spatial reference frame.

IV. EXPERIMENTS

Our experiments investigate pairwise distances between whole-brain MRI scans acquired from a diverse population with pairwise relationships including 1) close genetic links between siblings sharing 25-100% of their polymorphic genes and 2) broad genetic links between non-siblings sharing nominal genetic information due to sex and common racial ancestry. We hypothesize that closer genetic proximity will be reflected in higher pairwise similarity and thus lower Jaccard distance. We expect that pairwise distance based on our proposed soft set equivalence (SSE) $d_J(A, B) = -\log J_{SSE}(A, B)$ as defined in Equations (2) and (4) and our geometrical kernel as defined by Equations (9) and (10) will lead to improved identification of pairwise relationship labels.

A. Image Data and Preprocessing

Our test set consists of MRI scans of $N = 1010$ unique subjects with genetic ground truth from the Human Connectome Project Q4 release [4], aged 22-36 years (mean 29 years), 468 males and 542 females, from 434 unique families. There are thus $N(N-1)/2 = 509,545$ pairwise relationships, where each pair of subjects is related by one of five possible sibling relationship labels $L = \{MZ, DZ, FS, HS, UR\}$ for monozygotic twins (MZ), dizygotic twins (DZ), full non-twin siblings (FS), half-siblings (HS) and unrelated non-siblings (UR), with respectively $\{134, 71, 607, 44, 509194\}$ unique pairs. Family relationship labels are based on mother and

father identity and zygosity (for twins), confirmed via genome-wide single nucleotide polymorphism (SNP) genotyping [65]. Note that evaluating the similarity of $N(N-1)/2$ pairwise relationships via brute force image registration, e.g. optimizing cross-correlation, quickly becomes computationally intractable as N grows large.

MRI data consist of skull-stripped T1w images from the HCP preprocessing pipeline with 0.7mm isotropic voxels, note that the method can be applied to other scalar image modalities (e.g. T2w, FA), all images are spatially registered to a MNI space template with a standard rigid transform, preserving individual brain size and shape [66]–[68]. Generic 3D SIFT-Rank features are extracted from MRI data, where geometry \bar{g}_i is identified as extrema of an difference-of-Gaussian scale-space [21] and local appearance is encoded as a 64-dimensional SIFT-Rank appearance descriptor \bar{a}_i . Feature extraction requires approximately 3 sec. / per image via a GPU implementation of 3D SIFT extraction [69], and results in an average of 1,400 features per image, for a total of 1,488,065 features. Approximate kNN correspondences between appearance descriptors are identified across the entire database using efficient KD-tree indexing [23], where lookup requires 0.8 sec. / subject for $k=200$ nearest neighbors on an i7-5600@2.60Ghz machine with 16 GB RAM (1.64 GB used).

B. Close genetic proximity: Siblings

Figure 3 shows distributions of pairwise Jaccard distance conditioned on pairwise relationships. Our proposed kernel based on appearance and geometry (Figure 3, in green) generally increases separation between different sibling relationships in comparison to appearance only (Figure 3, in orange) as in [24]. A two-tailed Kolmogorov-Smirnov test shows all distributions to be significantly different ($p\text{-value} < 1e-10$) except those of DZ and FS siblings sharing approximately 50% of their genes ($p\text{-value} = 0.0199$). Upon inspection, the highest Jaccard distance outliers were due to noticeable spatial misalignment of a small number of subjects (e.g. Figure 3 a). The lowest distance outliers indicate potential sibling relationships. The HCP dataset contains several subjects labeled as family unknown due to uncertain genotyping [65], where blue circles near Figure 3 b) indicates members of the families with the lowest average Jaccard distance to these subjects. As distances are within the expected sibling ranges, and zygosity and demographic information are consistent, it is likely these pairs represent actual sibling relationships, labeled differently due to genotyping uncertainty.

As sibling pairs exhibit significantly lower distance than UR pairs, we investigate the degree to which they can be distinguished from unrelated pairs based on a simple distance threshold. Figure 4 shows the Receiver Operating Characteristic (ROC) curves for sibling relationships based on distance, comparing hard set equivalence (HSE) with binary kernel vs. soft set equivalence (SSE) for appearance and geometry kernels. SSE for combined appearance and geometry kernels is always superior to HSE in terms of the area-under-curve (AUC) performance measure. Table I quantifies the improvement of SSE vs HSE, for various numbers of keypoint

nearest neighbors (20, 100, 200), where the highest AUC values are obtained for SSE with 200 NN correspondences. HSE is noticeably sensitive to the number of NNs, and the classification performance generally decrease number of NNs. In contrast, the SSE is relatively stable and generally increases with the number of NNs used.

C. Distant genetic proximity: unrelated subjects

Unrelated (UR) subject pairs share nominal amounts of genetic information, with subtle similarities due to demographic factors such as common sex and ancestral race. We thus expect whole-brain distance to be lowest for pairs of the same race and sex (R,S), highest for different race and sex (\bar{R},\bar{S}), and intermediate for either same race (R, \bar{S}) or sex (\bar{R} ,S). While the mean distances for conditional distributions in Figure 5 generally increase with differences in demographic labels, there are many exceptions where pairs with different labels exhibit lower distance than those with the same labels. We note this is consistent with pairwise genetic differences, where pairs of unrelated individuals from different populations may often exhibit higher genetic similarity than those from the same population [70].

Age difference between subjects is a potential confound in whole brain Jaccard distance. Figure 6 plots the variation in distance vs. age difference. Distance distributions are virtually identical across the HCP subject age range spanning 22-36 years of age, indicating that age difference is not a major confound in this relatively young HCP cohort where brain morphology is relatively stable. Note that the Jaccard distance was found to increase with age difference in older subjects due to natural aging and neurodegenerative disease in [10], similarly in rapid neurodevelopment over the infant range in [71].

D. Group Prediction: Sex

While pairwise Jaccard distance is highly informative regarding sibling relationships, it is insufficient for predicting group labels such as sex, age or disease. A simple modification can be used to predict group labels, by evaluating the distance between a single keypoint set A and supersets formed by the union of group members (excluding subject A), e.g. keypoints for *all Males* $d_J(A, \mathcal{M})$ and *all Females* $d_J(A, \mathcal{F})$. Supersets \mathcal{M} and \mathcal{F} are solely composed of unrelated subjects to overcome biases due to family relationships. These distances are combined in a basic linear classifier with a single threshold parameter τ to adjust for differences in the numbers of keypoints per group based on the following equation:

$$\text{Class}(A) = \begin{cases} \text{Female} & \text{if } d_J(A, \mathcal{F}) - d_J(A, \mathcal{M}) + \tau > 0 \\ \text{Male} & \text{otherwise.} \end{cases} \quad (11)$$

Figure 7 shows ROCs curves for sex prediction obtained by varying τ over the range $[-\infty, \infty]$, comparing Jaccard distance computed with binary, appearance only and combined appearance and geometry kernels. A possible confound is brain size, which is on average slightly larger for males than females[72].

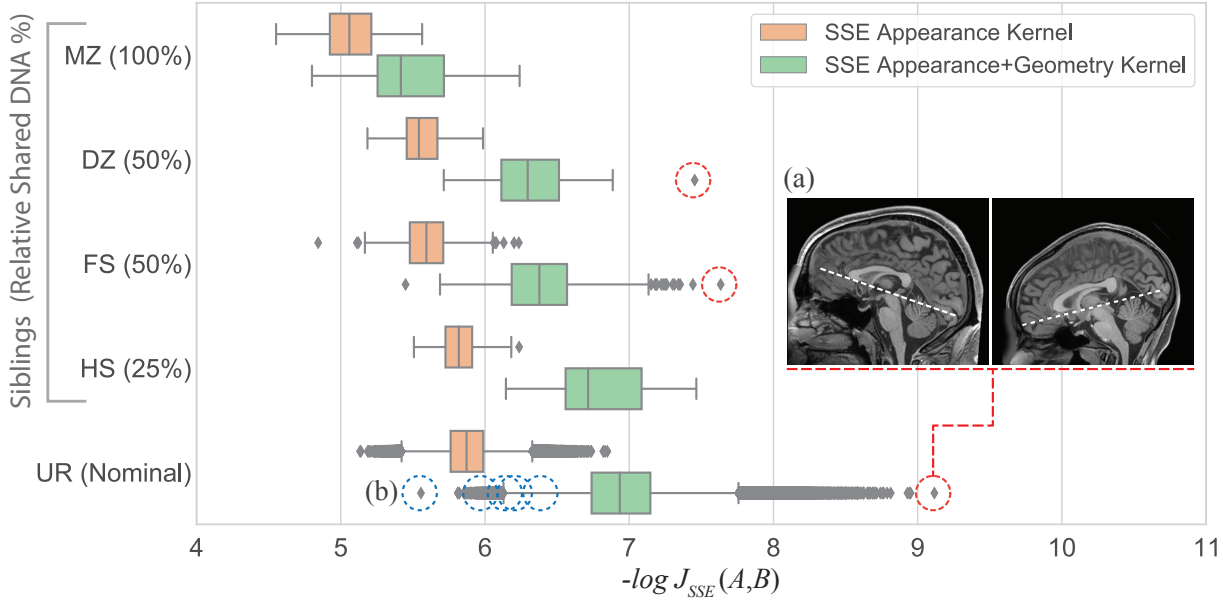


Fig. 3. Distributions of Jaccard distances $-\log J_{SSE}(A, B)$ conditioned on pairwise labels $L = \{MZ, DZ, FS, HS, UR\}$, comparing kernels with and without geometry (green vs. orange). Note that the distance generally increases with genetic separation, and that geometrical kernels increase separation between sibling relationship labels. Outlier pairs can be easily identified and inspected for irregularity, (a) unusually high distances (red circles) generally indicate spatial misalignment (b) low distances indicate unusually close, potentially valid sibling relationships, with blue circles being pairs with unknown family labels due to uncertain genotyping [65]

Kernel \ Label	$k = 20$			$k = 100$			$k = 200$		
	HSE_{Binary}	$SSE_{App.}$	$SSE_{App.} + Geo.$	HSE_{Binary}	$SSE_{App.}$	$SSE_{App.} + Geo.$	HSE_{Binary}	$SSE_{App.}$	$SSE_{App.} + Geo.$
Monozygotic	0.9983	0.9993	0.9996	0.9544	0.9995	0.9998	0.9272	0.9994	0.9999
Dizygotic	0.8922	0.8825	0.9044	0.8018	0.9034	0.9250	0.7541	0.9181	0.9391
Full-Sibling	0.8423	0.8433	0.8753	0.7611	0.8569	0.8888	0.7358	0.8680	0.8989

TABLE I

AREA UNDER THE CURVE (AUC) VALUES FOR SIBLING PAIR CLASSIFICATION, COMPARING KERNELS AND NUMBERS OF NEAREST NEIGHBORS (K). COMBINED APPEARANCE AND GEOMETRY KERNELS BASED ON SSE CONSISTENTLY OUTPERFORM APPEARANCE AND BINARY (HSE) KERNELS.

As the appearance kernel is invariant to image scale, the $AUC=0.93$ reflects prediction accuracy independently of image size. Our proposed combined approach achieves the highest $AUC=0.97$, again outperforming other options.

V. DISCUSSION

In this paper we propose a novel, highly specific distance measure for pairwise volumetric image matching. Given images represented as localized keypoint sets, we propose generalizing the Jaccard index to account for soft equivalence between pairs of keypoint sets. A novel kernel estimator is proposed to model keypoint geometry in terms of location and scale within the image. The soft Jaccard index is used as a distance measure to predict 509,545 pairwise relationship labels between MRI brain scans of 1010 subjects, including siblings and twins, and significantly improves upon previous technologies [10], [13]. To our knowledge, we report the highest recall rates for family members in T1w brain scans, where monozygotic twins can be identified with virtually perfect accuracy. A minor modification allows the Jaccard distance to predict group labels such as sex with high accuracy.

Our method adopts a memory-based model that leverages keypoint information from all images, and is thus well-suited for curating large medical image datasets. Highly robust, efficient and general algorithms for keypoint extraction and indexing [73] allow fine-grained image-to-image comparisons for arbitrarily large datasets with minimal preprocessing. Outliers due to geometric misalignment or potentially incorrect pairwise relationships may be identified via unusually high or low Jaccard distance. Previous work identified mislabelled scans of individuals in various large neuroimage datasets as well as image artifacts [10], here our improved method allows us to identify several instances of family members undetected by genotyping [65], based solely on brain MRI data. This, to our knowledge, has never been reported, and the Human Connectome Project has confirmed our findings of several cases. With these capabilities our method promises to be a highly useful tool for accurately curating large medical image datasets for precision medicine and research purposes.

The task of pairwise relationship prediction can be viewed as the finest grain of categorization, where the number of unique pairwise relationship labels is linear $O(N)$ in the number of data N , e.g. 434 families from $N=1010$ images, as

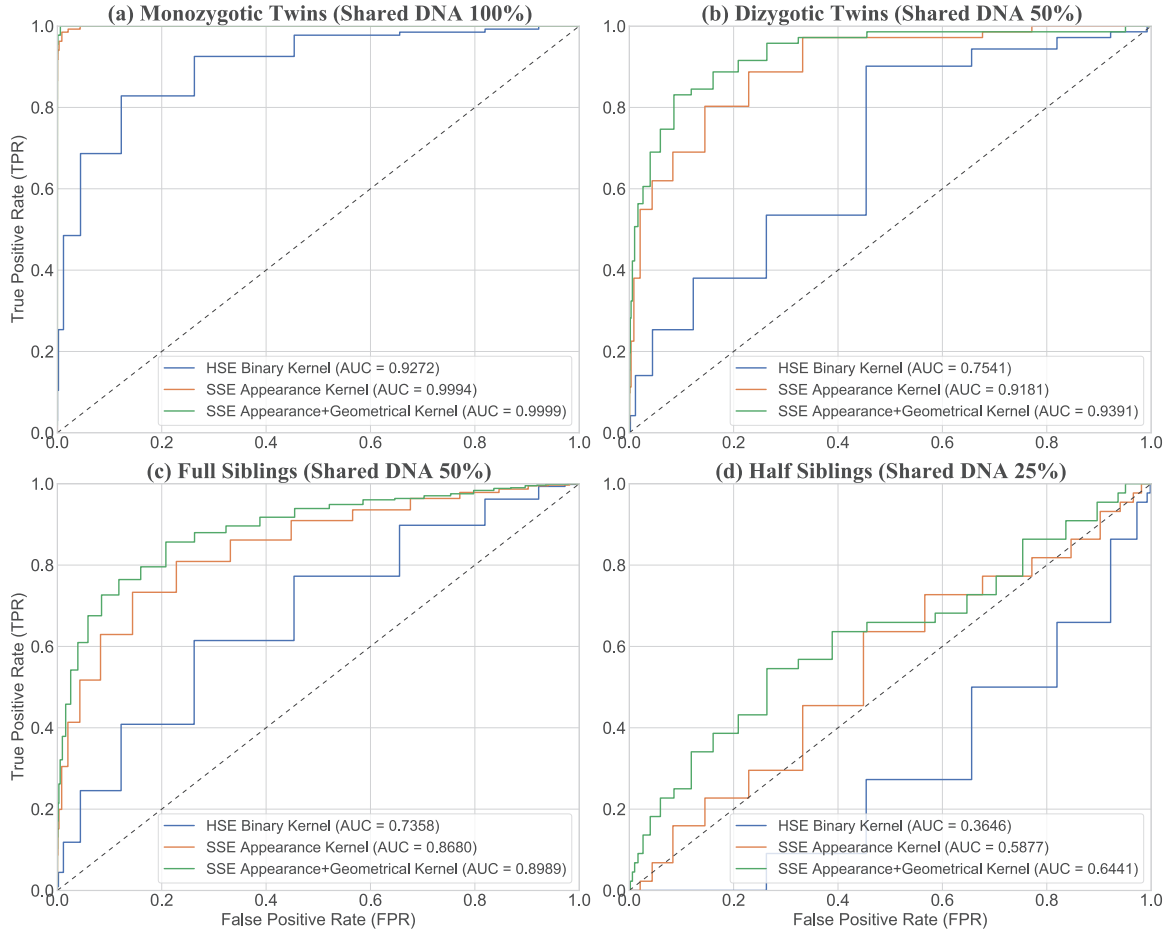


Fig. 4. ROC curves for sibling identification based on Jaccard distance for (a) MZ, (b) DZ, (c) FS and (d) HS pairs. Curves compare hard set equivalence (HSE) vs. the proposed soft set equivalence (SSE) for three values of nearest neighbor (NN) keypoint correspondences (NN=20,100,200). Combined appearance and geometrical kernels outperform appearance and binary kernels in terms of classification performance.

opposed to group classification where all data are associated with a small number of labels (e.g. male, female). Pairwise prediction thus represents a challenge for recent deep Convolutional Neural Networks (CNN) methods which generally require large numbers of training data per category. In future work, generic 3D SIFT keypoint correspondences here could potentially be used to train domain-specific keypoint models [35], [37], as they may be used to identify correspondences in arbitrary modalities or anatomies without training. Auto-encoders, such as anomaly detection, could potentially be adapted to generate subject-specific codes between pairs of images [74]. Analysis beyond pairs of subjects could be generalized via graph theory and clique structure of families [75]. All code required to reproduce our results may be obtained at <https://github.com/3dsift-rank/3DSIFT-Rank>.

REFERENCES

- [1] M. A. Hamburg and F. S. Collins, "The path to personalized medicine," *New England Journal of Medicine*, vol. 363, no. 4, pp. 301–304, 2010.
- [2] G. J. Annas and S. Elias, "23andme and the fda," *New England Journal of Medicine*, vol. 370, no. 11, pp. 985–988, 2014.
- [3] . G. P. Consortium *et al.*, "A global reference for human genetic variation," *Nature*, vol. 526, no. 7571, pp. 68–74, 2015.
- [4] D. Van Essen, K. Ugurbil, E. Auerbach, D. Barch, T. Behrens, R. Bucholz, A. Chang, L. Chen, M. Corbetta, S. Curtiss, S. Della Penna, D. Feinberg, M. Glasser, N. Harel, A. Heath, L. Larson-Prior, D. Marcus, G. Michalareas, S. Moeller, R. Oostenveld, S. Petersen, F. Prior, B. Schlaggar, S. Smith, A. Snyder, J. Xu, and E. Yacoub, "The Human Connectome Project: A data acquisition perspective," *NeuroImage*, vol. 62, no. 4, pp. 2222–2231, 10 2012.
- [5] S. Gerber, T. Tasdizen, P. Thomas Fletcher, S. Joshi, R. Whitaker, and Alzheimer's Disease Neuroimaging Initiative (ADNI), "Manifold modeling for brain population analysis," *Medical Image Analysis (MIA)*, vol. 14, no. 5, pp. 643–53, 10 2010.
- [6] T. Brosch, P. Gmbh, I. Technologies, and R. Tam, "Manifold Learning of Brain MRIs by Deep Learning Manifold Learning of Brain MRIs," *International Conference on Medical Image Computing and Computer-Assisted Intervention (MICCAI)*, vol. 16, no. September, 2015.
- [7] Y. Ono, E. Trulls, P. Fua, and K. Moo Yi, "LF-Net: Learning Local Features from Images," in *Advances in Neural Information Processing Systems (NeurIPS)*, 2018.
- [8] M. Levandowsky and D. Winter, "Distance between sets," *Nature*, vol. 234, no. 5323, p. 34, 11 1971.
- [9] M. Toews and W. Wells, "How are siblings similar? How similar are siblings? Large-scale imaging genetics using local image features," in *International Symposium on Biomedical Imaging (ISBI)*, IEEE. IEEE, 4 2016, pp. 847–850.
- [10] L. Chauvin, K. Kumar, C. Wachinger, M. Vangel, J. de Guise, C. Desrosiers, W. Wells, M. Toews, and Alzheimer's Disease Neuroimaging Initiative (ADNI), "Neuroimage signature from salient key-points is highly specific to individuals and shared by close relatives," *NeuroImage*, vol. 204, no. 20, 9 2020.
- [11] M. Toews and W. Wells, "Efficient and robust model-to-image alignment

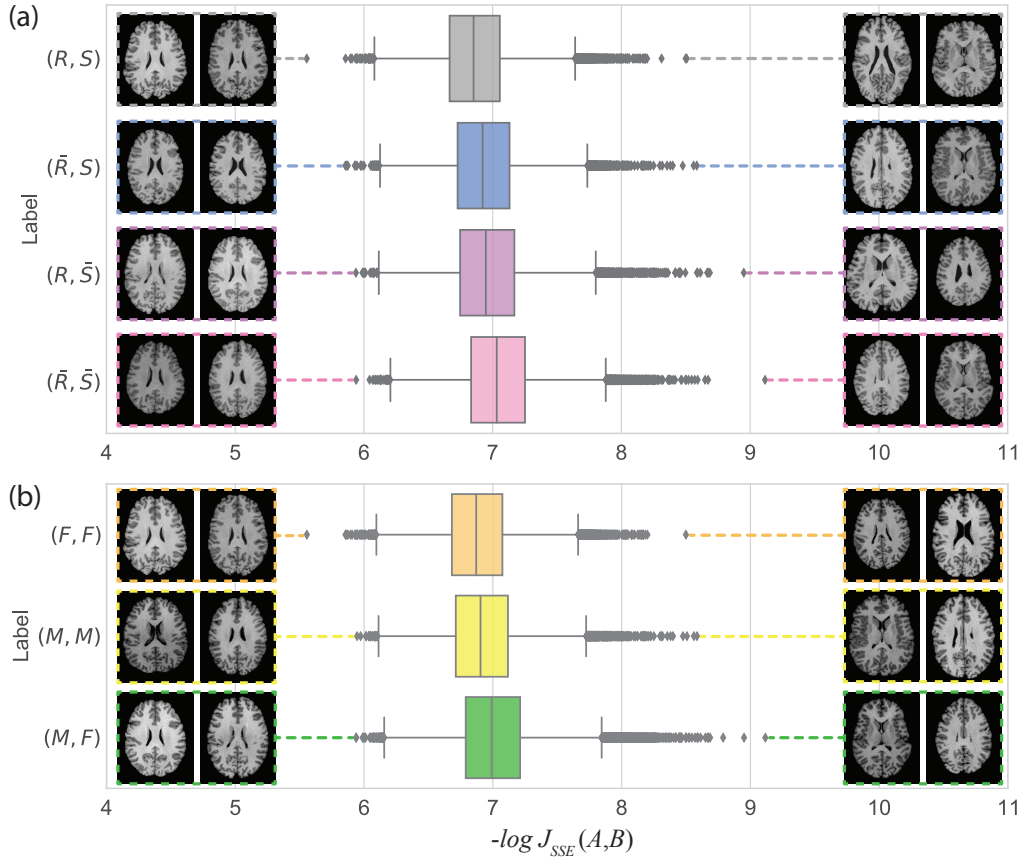


Fig. 5. Jaccard distance $-\log J_{SSE}(A, B)$ distributions between unrelated pairs conditioned on shared demographic information. **(a)** same race, same sex (R, S) ; different race, same sex (\bar{R}, S) ; same race, different sex (R, \bar{S}) , and different race, different sex (\bar{R}, \bar{S}) and **(b)** Female-Female (F, F) , Male-Male (M, M) , Male-Female (M, F) . Image pairs corresponding to minimum and maximum distances for each distribution are shown for visualization.

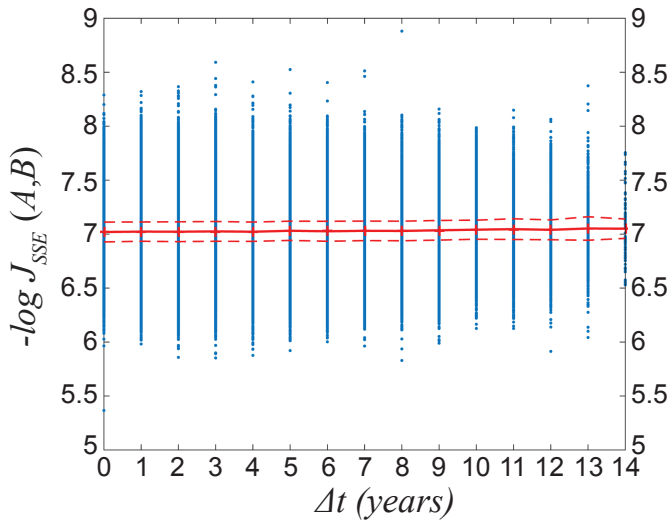


Fig. 6. Distributions of Jaccard distance $-\log J_{SSE}(A, B)$ conditioned on age difference Δt between unrelated pairs (A, B) conditioned on age difference Δt . The mean (solid red line) and standard deviation (dashed red lines) are plotted for each Δt . Age difference has no significant impact on the distance for unrelated healthy young adult brains (age 22-36 years), eliminating a possible confounding factor.

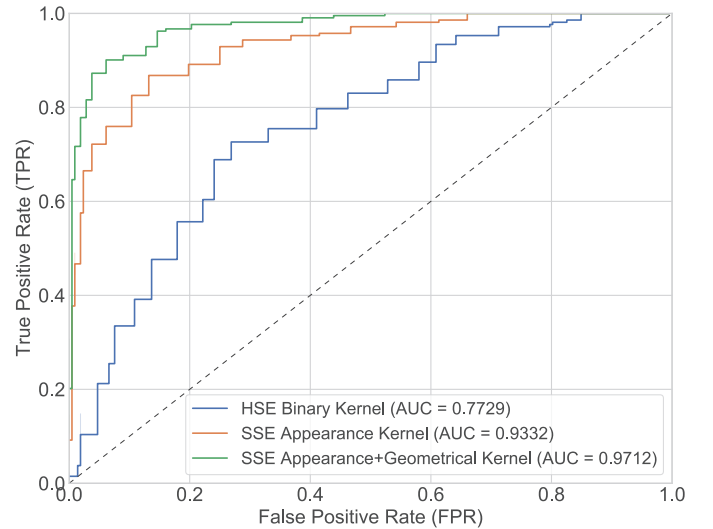


Fig. 7. ROC curves and AUC for sex prediction based on individual-to-group Jaccard distance, comparing binary, appearance only, and combined appearance and geometry kernels.

- [14] D. S. Marcus, T. H. Wang, J. Parker, J. G. Csernansky, J. C. Morris, and R. L. Buckner, "Open Access Series of Imaging Studies (OASIS): cross-sectional MRI data in young, middle aged, nondemented, and demented older adults," *Journal of cognitive neuroscience*, vol. 19, no. 9, pp. 1498–1507, 9 2007.
- [15] C. R. Jack Jr, M. A. Bernstein, N. C. N. Fox, P. Thompson, G. Alexander, D. Harvey, B. Borowski, P. J. Britson, J. L. Whitwell, C. Ward, others, C. R. C. Jack, M. A. Bernstein, N. C. N. Fox, P. Thompson, G. Alexander, D. Harvey, B. Borowski, P. J. Britson, J. L. Whitwell, C. Ward, A. M. Dale, J. P. Felmlee, J. L. Gunter, D. L. Hill, R. Killiany, N. Schuff, S. Fox-Bosetti, C. Lin, C. Studholme, C. S. DeCarli, G. Gunnar Krueger, H. A. Ward, G. J. Metzger, K. T. Scott, R. Mallozzi, D. Blezek, J. Levy, J. P. Debbins, A. S. Fleisher, M. Albert, R. Green, G. Bartzokis, G. Glover, J. Mugler, M. W. Weiner, H. A. Gunnar Krueger, H. A. Ward, G. J. Metzger, K. T. Scott, R. Mallozzi, D. Blezek, J. Levy, J. P. Debbins, A. S. Fleisher, M. Albert, R. Green, G. Bartzokis, G. Glover, J. Mugler, and M. W. Weiner, "The Alzheimer's disease neuroimaging initiative (ADNI): MRI methods," *Journal of the International Society for Magnetic Resonance in Medicine (ISMRM)*, vol. 27, no. 4, pp. 685–691, 4 2008.
- [16] D. C. Van Essen, S. M. Smith, D. M. Barch, T. E. J. Behrens, E. Yacoub, K. Ugurbil, W.-M. H. C. P. Consortium, and others, "The WU-Minn human connectome project: an overview," *NeuroImage*, vol. 80, pp. 62–79, 10 2013.
- [17] L. Chauvin, K. Kumar, C. Desrosiers, J. De Guise, W. Wells, and M. Toews, "Analyzing Brain Morphology on the Bag-of-Features Manifold," in *International Conference on Information Processing in Medical Imaging (IPMI)*, vol. 11492 LNCS. Springer Verlag, 2019, pp. 45–56.
- [18] M. R. Sabuncu, T. Ge, A. J. Holmes, J. W. Smoller, R. L. Buckner, B. Fischl, and Alzheimer's Disease Neuroimaging Initiative (ADNI), "Morphometricity as a measure of the neuroanatomical signature of a trait," *Proceedings of the National Academy of Sciences (PNAS)*, vol. 113, no. 39, pp. E5749–E5756, 9 2016.
- [19] O. Boiman, E. Shechtman, and M. Irani, "In defense of nearest-neighbor based image classification," in *Proceedings of the IEEE Conference on Computer Vision and Pattern Recognition (CVPR)*. IEEE, 2008, pp. 1–8.
- [20] T. Cover and P. Hart, "Nearest neighbor pattern classification," *IEEE Transactions on Information Theory (TIT)*, vol. 13, no. 1, pp. 21–27, 1 1967.
- [21] D. G. Lowe, "Distinctive image features from scale-invariant keypoints," *International Journal of Computer Vision (IJCV)*, vol. 60, no. 2, pp. 91–110, 11 2004.
- [22] T. Lindeberg, "Feature Detection with Automatic Scale Selection," *International Journal of Computer Vision (IJCV)*, vol. 30, no. 2, pp. 79–116, 1998.
- [23] M. Muja and D. Lowe, "Scalable nearest neighbor algorithms for high dimensional data," *IEEE Transactions on Pattern Analysis and Machine Intelligence (TPAMI)*, 2014.
- [24] L. Chauvin, K. Kumar, C. Wachinger, M. Vangel, J. de Guise, C. Desrosiers, W. Wells, M. Toews, A. D. N. Initiative *et al.*, "Neuroimage signature from salient keypoints is highly specific to individuals and shared by close relatives," *NeuroImage*, vol. 204, p. 116208, 2020.
- [25] M. Toews, C. Wachinger, R. S. J. Estepar, and W. Wells, "A Feature-Based Approach to Big Data Analysis of Medical Images," *International Conference on Information Processing in Medical Imaging (IPMI)*, vol. 24, pp. 339–350, 2015.
- [26] E. Marczewski and H. Steinhaus, "On a certain distance of sets and the corresponding distance of functions," in *Colloquium Mathematicum*, vol. 6, no. 1. Institute of Mathematics Polish Academy of Sciences, 1958, pp. 319–327.
- [27] D. Bajusz, A. Rácz, and K. Héberger, "Why is Tanimoto index an appropriate choice for fingerprint-based similarity calculations?" *Journal of Cheminformatics*, vol. 7, no. 1, 12 2015.
- [28] D. J. Rogers and T. T. Tanimoto, "A Computer Program for Classifying Plants," pp. 1115–1118.
- [29] Y. Yuan, M. Chao, and Y. C. Lo, "Automatic Skin Lesion Segmentation Using Deep Fully Convolutional Networks with Jaccard Distance," *IEEE Transactions on Medical Imaging (TMI)*, vol. 36, no. 9, 2017.
- [30] D. Molodtsov, "Soft set theory—first results," *Computers & Mathematics with Applications*, vol. 37, no. 4-5, pp. 19–31, 1999.
- [31] J. H. Park, O. H. Kim, and Y. C. Kwun, "Some properties of equivalence soft set relations," *Computers & Mathematics with Applications*, vol. 63, no. 6, pp. 1079–1088, 2012.
- [32] A. Gardner, J. Kanno, C. A. Duncan, and R. Selmic, "Measuring Distance Between Unordered Sets of Different Sizes," in *Proceedings of the IEEE Conference on Computer Vision and Pattern Recognition (CVPR)*, 2014, pp. 137–143.
- [33] O. Chum, J. Philbin, and A. Zisserman, "Near Duplicate Image Detection: min-Hash and tf-idf Weighting," in *The British Machine Vision Conference (BMVC)*, 2008.
- [34] D. Mukherjee, Q. M. Jonathan Wu, and G. Wang, "A comparative experimental study of image feature detectors and descriptors," *Machine Vision and Applications*, vol. 26, no. 4, pp. 443–466, 5 2015.
- [35] K. M. Yi, E. Trulls, V. Lepetit, and P. Fua, "LIFT: Learned invariant feature transform," in *Proceedings of the European Conference on Computer Vision (ECCV)*, vol. 9910 LNCS. Springer Verlag, 2016, pp. 467–483.
- [36] M. J. Tyszkiewicz, P. Fua, and E. Trulls, "DISK: Learning local features with policy gradient," in *Advances in Neural Information Processing Systems (NeurIPS)*, 2020.
- [37] D. Detone, T. Malisiewicz, and A. Rabinovich, "SuperPoint: Self-Supervised Interest Point Detection and Description," in *Proceedings of the IEEE Conference on Computer Vision and Pattern Recognition (CVPR) Workshops*, 2018.
- [38] A. Krizhevsky, I. Sutskever, and G. E. Hinton, "ImageNet Classification with Deep Convolutional Neural Networks," *Advances In Neural Information Processing Systems (NeurIPS)*, pp. 1–9, 2012.
- [39] M. Toews and W. Wells, "Sift-rank: Ordinal description for invariant feature correspondence," in *Proceedings of the IEEE Conference on Computer Vision and Pattern Recognition (CVPR)*, 2009, pp. 172–177.
- [40] J. Dong and S. Soatto, "Domain-size pooling in local descriptors: DSP-SIFT," *Proceedings of the IEEE Conference on Computer Vision and Pattern Recognition (CVPR)*, 2015.
- [41] R. Arandjelović and A. Zisserman, "Three things everyone should know to improve object retrieval," *Proceedings of the IEEE Conference on Computer Vision and Pattern Recognition (CVPR)*, 2012.
- [42] Y. Ke and R. Sukthankar, "PCA-SIFT: A more distinctive representation for local image descriptors," *Proceedings of the IEEE Conference on Computer Vision and Pattern Recognition (CVPR)*, 2004.
- [43] V. Balntas, K. Lenc, A. Vedaldi, and K. Mikolajczyk, "HPatches: A benchmark and evaluation of handcrafted and learned local descriptors," in *Proceedings of the IEEE Conference on Computer Vision and Pattern Recognition (CVPR)*, 2017.
- [44] J. L. Schönberger, H. Hardmeier, T. Sattler, and M. Pollefeys, "Comparative Evaluation of Hand-Crafted and Learned Local Features," in *Proceedings of the IEEE Conference on Computer Vision and Pattern Recognition (CVPR)*, 2017.
- [45] I. Machado, M. Toews, J. Luo, P. Unadkat, W. Essayed, E. George, P. Teodoro, H. Carvalho, J. Martins, P. Golland, S. Pieper, S. Frisken, A. Golby, and W. Wells, "Non-rigid registration of 3D ultrasound for neurosurgery using automatic feature detection and matching," *International Journal of Computer Assisted Radiology and Surgery (IJCARS)*, vol. 13, no. 10, pp. 1525–1538, 10 2018.
- [46] C. Wachinger, M. Toews, G. Lings, W. Wells, and P. Golland, "Key-point transfer for fast whole-body segmentation," *IEEE Transactions on Medical Imaging (TMI)*, 2018.
- [47] R. Geirhos, C. Michaelis, F. A. Wichmann, P. Rubisch, M. Bethge, and W. Brendel, "Imagenet-trained CNNs are biased towards texture; increasing shape bias improves accuracy and robustness," in *International Conference on Learning Representations (ICLR)*, 2019.
- [48] C. Wachinger, P. Golland, W. Kremen, B. Fischl, M. Reuter, A. D. N. Initiative, and others, "BrainPrint: A discriminative characterization of brain morphology," *NeuroImage*, vol. 109, pp. 232–248, 4 2015.
- [49] K. Kumar, C. Desrosiers, K. Siddiqi, O. Colliot, and M. Toews, "Fiberprint: A subject fingerprint based on sparse code pooling for white matter fiber analysis," *NeuroImage*, vol. 158, pp. 242–259, 9 2017.
- [50] G. L. Colclough, S. M. Smith, T. E. Nichols, A. M. Winkler, S. N. Sotiropoulos, M. F. Glasser, D. C. Van Essen, and M. W. Woolrich, "The heritability of multi-modal connectivity in human brain activity," *eLife*, vol. 6, p. e20178, 7 2017.
- [51] E. S. Finn, X. Shen, D. Scheinost, M. D. Rosenberg, J. Huang, M. M. Chun, X. Papademetris, and R. T. Constable, "Functional connectome fingerprinting: identifying individuals using patterns of brain connectivity," *Nature neuroscience*, vol. 18, no. 11, pp. 1664–71, 11 2015.
- [52] M. Reuter, F.-E. Wolter, and N. Peinecke, "Laplace–Beltrami spectra as 'Shape-DNA' of surfaces and solids," *Computer-Aided Design*, vol. 38, no. 4, pp. 342–366, 4 2006.
- [53] S. A. Valizadeh, F. Liem, S. Mérillat, J. Hänggi, and L. Jäncke, "Identification of individual subjects on the basis of their brain anatomical features," *Scientific reports*, vol. 8, no. 1, p. 5611, 12 2018.
- [54] C. Sudlow, J. Gallacher, N. Allen, V. Beral, P. Burton, J. Danesh, P. Downey, P. Elliott, J. Green, M. Landray, B. Liu, P. Matthews, G. Ong,

- J. Pell, A. Silman, A. Young, T. Sprosen, T. Peakman, and R. Collins, "UK Biobank: An Open Access Resource for Identifying the Causes of a Wide Range of Complex Diseases of Middle and Old Age," *PLOS Medicine*, vol. 12, no. 3, p. e1001779, 3 2015.
- [55] P. M. Thompson, T. D. Cannon, K. L. Narr, T. Van Erp, V.-P. Poutanen, M. Huttunen, J. Lönqvist, C.-G. Standertskjöld-Nordenstam, J. Kaprio, M. Khaledy, R. Dail, C. I. Zoumalan, A. W. Toga, and others, "Genetic influences on brain structure," *Nature neuroscience*, vol. 4, no. 12, p. 1253, 12 2001.
- [56] S. J. van der Lee, G. V. Roshchupkin, H. H. Adams, H. Schmidt, E. Hofer, Y. Saba, R. Schmidt, A. Hofman, N. Amin, C. M. van Duijn, M. W. Vernooij, M. A. Ikram, and W. J. Niessen, "Gray matter heritability in family-based and population-based studies using voxel-based morphometry," *Human Brain Mapping (HBM)*, vol. 38, no. 5, 2017.
- [57] H. Jegou, F. Perronnin, M. Douze, J. Sánchez, P. Pérez, and C. Schmid, "Aggregating local image descriptors into compact codes," in *IEEE Transactions on Pattern Analysis and Machine Intelligence (TPAMI)*, 2010.
- [58] P. F. Felzenszwalb, R. B. Girshick, D. McAllester, and D. Ramanan, "Object detection with discriminatively trained part-based models," *IEEE Transactions on Pattern Analysis and Machine Intelligence (TPAMI)*, vol. 32, no. 9, 2010.
- [59] G. Csurka, C. Dance, L. Fan, J. Willamowski, and C. Bray, "Visual categorization with bags of keypoints," *Proceedings of the European Conference on Computer Vision (ECCV) Workshops*, 2004.
- [60] M. Toews, W. Wells, D. L. Collins, and T. Arbel, "Feature-based morphometry: Discovering group-related anatomical patterns," *NeuroImage*, vol. 49, no. 3, pp. 2318–2327, 2010.
- [61] M. R. Kiley and M. S. Hossain, "Who are my family members? a solution based on image processing and machine learning," *International Journal of Image and Graphics*, vol. 20, no. 04, p. 2050033, 2020.
- [62] B. Ahmad, M. Usama, J. Lu, W. Xiao, J. Wan, and J. Yang, "Deep convolutional neural network using triplet loss to distinguish the identical twins," in *2019 IEEE Globecom Workshops (GC Wkshps)*. IEEE, 2019, pp. 1–6.
- [63] F. Juefei-Xu and M. Savvides, "An augmented linear discriminant analysis approach for identifying identical twins with the aid of facial asymmetry features," in *Proceedings of the IEEE Conference on Computer Vision and Pattern Recognition (CVPR)*, 2013.
- [64] J. R. Paone, P. J. Flynn, P. J. Phillips, K. W. Bowyer, R. W. Bruegge, P. J. Grother, G. W. Quinn, M. T. Pruitt, and J. M. Grant, "Double trouble: Differentiating identical twins by face recognition," *IEEE Transactions on Information Forensics and Security (TIFS)*, vol. 9, no. 2, 2014.
- [65] H. WU-Minn, "1200 subjects data release reference manual," 2017. [Online]. Available: <https://www.humanconnectome.org>
- [66] M. F. Glasser, S. N. Sotiropoulos, J. A. Wilson, T. S. Coalson, B. Fischl, J. L. Andersson, J. Xu, S. Jbabdi, M. Webster, J. R. Polimeni, D. C. Van Essen, and M. Jenkinson, "The minimal preprocessing pipelines for the Human Connectome Project," *NeuroImage*, vol. 80, pp. 105–124, 10 2013.
- [67] M. Jenkinson, P. Bannister, M. Brady, and S. Smith, "Improved Optimization for the Robust and Accurate Linear Registration and Motion Correction of Brain Images," *NeuroImage*, 2002.
- [68] M. Jenkinson and S. Smith, "A global optimisation method for robust affine registration of brain images," *Medical Image Analysis (MIA)*, vol. 5, no. 2, 2001.
- [69] É. Pepin, J.-B. Carlier, L. Chauvin, M. Toews, and R. Harmouche, "Large-scale unbiased neuroimage indexing via 3d gpu-sift filtering and keypoint masking," in *Machine Learning in Clinical Neuroimaging and Radiogenomics in Neuro-oncology*. Springer, 2020, pp. 108–118.
- [70] D. J. Witherspoon, S. Wooding, A. R. Rogers, E. E. Marchani, W. S. Watkins, M. A. Batzer, and L. B. Jorde, "Genetic similarities within and between human populations," *Genetics*, vol. 176, no. 1, pp. 351–359, 2007.
- [71] M. Toews, W. Wells, and L. Zöllei, "Feature-based developmental model of the infant brain in structural MRI," in *International Conference on Medical Image Computing and Computer-Assisted Intervention (MICCAI)*, vol. 7511 LNCS, 2012.
- [72] L. Eliot, A. Ahmed, H. Khan, and J. Patel, "Dump the 'dimorphism': Comprehensive synthesis of human brain studies reveals few male-female differences beyond size," 2020.
- [73] M. Toews, L. Zöllei, and W. Wells, "Feature-based alignment of volumetric multi-modal images," in *International Conference on Information Processing in Medical Imaging (IPMI)*, vol. 23. Springer, 2013, pp. 25–36.
- [74] C. Baur, S. Denner, B. Wiestler, N. Navab, and S. Albarqouni, "Autoencoders for unsupervised anomaly segmentation in brain MR images: A comparative study," *Medical Image Analysis (MIA)*, vol. 69, 4 2021.
- [75] J. R. Blair and B. Peyton, "An introduction to chordal graphs and clique trees," in *Graph theory and sparse matrix computation*. Springer, 1993, pp. 1–29.

ACKNOWLEDGMENT

Data were provided in part by the Human Connectome Project, WU-Minn Consortium (Principal Investigators: David Van Essen and Kamil Ugurbil; 1U54MH091657) funded by the 16 NIH Institutes and Centers that support the NIH Blueprint for Neuroscience Research; and by the McDonnell Center for Systems Neuroscience at Washington University.

This work was supported by NIH grant P41EB015902 (NAC), the Quebec (FRQNT) New Researchers Startup Program and the Canadian National Sciences and Research Council (NSERC) Discovery Grant.